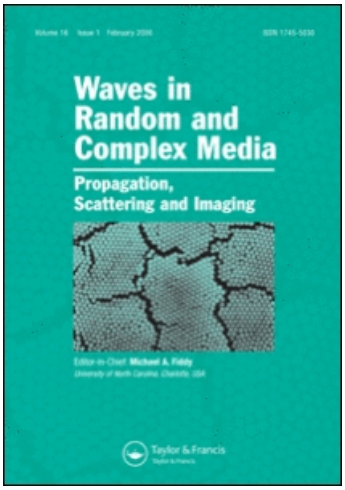

Waves in Random and Complex Media
Publication details, including instructions for authors and subscription information:
http://www.informaworld.com/smpp/title~content=t716100762

Scattering from canonical objects above a sea-like one-dimensional rough surface from a rigorous fast method

G. Kubické [a]; C. Bourlier [a]; J. Saillard [a]
[a] IREENA Laboratory, Fédération CNRS Atlanstic, Université de Nantes, Polytech'Nantes, La Chantrerie, 44306 Nantes Cedex 3, France

Online publication date: 29 January 2010

To cite this Article Kubické, G., Bourlier, C. and Saillard, J.(2010) 'Scattering from canonical objects above a sea-like one-dimensional rough surface from a rigorous fast method', Waves in Random and Complex Media, 20: 1, 156 — 178
To link to this Article: DOI: 10.1080/17455030903476712
URL: http://dx.doi.org/10.1080/17455030903476712

Waves in Random and Complex Media
Vol. 20, No. 1, February 2010, 156–178

Taylor & Francis
Taylor & Francis Group

Scattering from canonical objects above a sea-like one-dimensional rough surface from a rigorous fast method

G. Kubické*, C. Bourlier and J. Saillard

IREENA Laboratory, Fédération CNRS Atlanstic, Université de Nantes, Polytech'Nantes, La Chantrerie, Rue C. Pauc, BP 50609, 44306 Nantes Cedex 3, France

(*Received 1 April 2009; final version received 1 November 2009*)

This paper is devoted to scattering from a canonical object above a sea-like one-dimensional rough surface (two-dimensional problem). Such a problem involves a high number of unknowns and cannot be solved easily with a Method of Moments by using a direct LU inversion. Thus, a recently developed fast numerical method called Extended-PILE combined with FB-SA is used. First, a parametrization is proposed for the FB-SA by considering the sea surface only. Then, the convergence of E-PILE+FB-SA is tested for the scattering from a cylinder, a plate and a cross located above a rough surface obeying a Gaussian process with the Elfouhaily et al. spectrum. After generating several surface realizations, a Monte Carlo process is applied on the scattered fields in order to discuss on the Normalized Radar Cross-Section (NRCS) for a maritime application at microwave frequencies. Eventually, the study focuses on the case of low grazing incidence.

1. Introduction

The study of scattering from an object above a rough surface is a subject of great interest. The applications of such research concern many areas such as remote sensing, radar surveillance, optics and acoustics. Since the sea surface can be modeled as a rough surface, these applications are useful for the maritime domain in which some radar reflectors are used in several situations: mounted on a buoy to mark a shoal or mounted on a ship's mast, for example. Such a problem implies many parameters, such as incidence angle, frequency, shape and size of the reflector, position above the surface, and so on. Thus, some models are needed to design the radar reflectors. On a related subject, several asymptotic and exact models have been developed for scattering from an object below a rough surface [1–6] and on a rough surface (the object is partially buried) [7–9]. Recently, several studies have led to some asymptotic and exact numerical models for scattering from an object above a

*Corresponding author. Email: gildas.kubicke@univ-nantes.fr

ISSN 1745–5030 print/ISSN 1745–5049 online

DOI: 10.1080/17455030903476712
http://www.informaworld.com

rough surface [3,10–16]. But, in numerical simulations, the surface length plays an important role since a tapered wave is employed to eliminate the finite surface length edge effects [17,18]. Indeed, the tapered wave width should be large enough to respect the Helmholtz equation and to illuminate both the object and the surface and, as a result, the surface has to be large enough for the field to vanish at the surface extremities. So, it is interesting and necessary to investigate exact fast numerical methods to treat such a large problem.

On one hand, some exact fast numerical methods have been developed for a single rough surface (without the object). For instance, one can quote the Banded-Matrix-Iterative-Approach/CAnonical Grid (BMIA-CAG) of Tsang et al. [19,20] of complexity $\mathcal{O}(N_2 \log N_2)$, the Method of Ordered Multiple Interactions (MOMI) of Kapp et al. [21] of complexity $\mathcal{O}(N_2^2)$, the Forward–Backward (FB) method of Holliday et al. [22] of complexity $\mathcal{O}(N_2^2)$, and the accelerated version Forward–Backward Spectral Acceleration (FB-SA) of Chou et al. [23] of complexity $\mathcal{O}(N_2)$, in which N_2 is the number of unknowns on the rough surface. In [24] and [25], the FB and FB-SA methods have been extended to the case of a one-dimensional imperfect conducting rough surface by considering a high imaginary part of the permittivity, such as the sea surface at microwave frequencies.

On the other hand, Déchamps et al. [26] have recently developed a fast numerical method, PILE (Propagation-Inside-Layer Expansion), devoted to scattering by a stack of two one-dimensional interfaces separating homogeneous media, which corresponds to the problem depicted in Figure 1(a). The main advantage of the PILE method is that the resolution of the linear system (obtained from the Method of Moments: MoM) is broken up into different steps. Two steps are dedicated to solving for the local interactions, which can be done from efficient methods valid for a single rough interface, such FB-SA and BMIA/CAG, and two are dedicated to solving for the coupling interactions.

More recently, the PILE method has been applied by Bourlier et al. [27] to the problem depicted in Figure 1(b). Kubické et al. [28] have proposed the extended version of the PILE method, called E-PILE (Extended-PILE), in order to treat the more general case of two illuminated surfaces. This approach was used for scattering from a cylinder above a rough surface (obeying a Gaussian process with a Gaussian height spectrum) as depicted in Figure 1(c). In this case, the two surfaces are illuminated, unlike cases (a) and (b). In addition, to accelerate this method and to treat a large problem, the local interactions on the rough surface are computed from FB-SA. Since the number of unknowns on the rough surface is much greater than that on the object, the complexity of the method is then $\mathcal{O}(N_2)$.

In this paper, the E-PILE method combined with FB-SA (E-PILE+FB-SA) is applied to a more realistic scene made up of a canonical object (cylinder, plate and cross) above an ocean-like surface obeying the Elfouhaily et al. height spectrum [29]. Moreover, the Impedance Boundary Condition (IBC) is used since the sea surface is assumed to be highly conducting at radar microwave frequencies [30]. Studies are focused on the convergence of E-PILE+FB-SA for a maritime context. Numerical results are provided for a realistic scene by using a Monte Carlo process and the specific case of Low Grazing Angles (LGAs) is investigated.

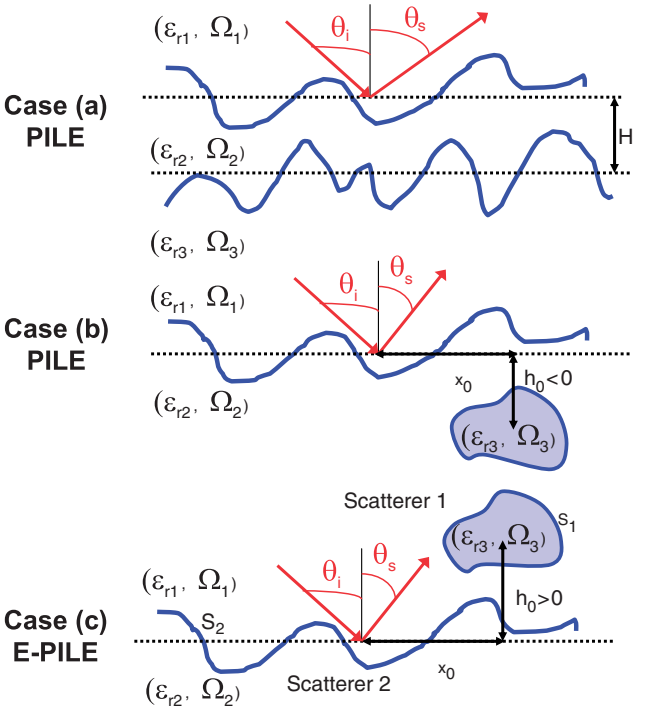

Figure 1. (Color online) Description of the problem. (a) Scattering by a *stack* of two rough interfaces separating homogeneous media. (b) Scattering by an object *below* a rough surface. (c) Scattering by an object *above* a rough surface. The media $\{\Omega_1, \Omega_2, \Omega_3\}$ of permittivities $\{\epsilon_{r1}, \epsilon_{r2}, \epsilon_{r3}\}$ are assumed to be homogeneous, and the scatterers are invariant along the direction normal to the figure.

The paper is organized as follows. In Section 2, a brief summary of the E-PILE method combined with FB-SA is given. In Section 3, the convergence of this approach is studied (with respect to the incidence angle θ_i, the wind speed above the sea u_{10}, and the sea surface length L_2) by considering first, the sea surface only. In the same way, the convergence of E-PILE+FB-SA is studied for scattering from canonical objects above a sea-like surface at microwave frequencies. In Section 4, the method is applied to a more realistic scene by using a Monte Carlo process for a cross located above a sea-like surface at microwave frequencies. Comparisons with results obtained by considering a single rough surface (without the object) and by considering a cross above a flat surface permit us to study the coupling between the surface and the object and the roughness effect. Finally, Section 4 focuses on the case of low grazing incidence.

Such a study of the convergence and parametrization of the FB-SA for a sea surface, and its efficient use in the E-PILE algorithm, have never been done before. Thus, E-PILE+FB-SA allows us to obtain interesting new and more realistic results, in particular near low grazing incidence.

2. A summary of the E-PILE combined with FB-SA

2.1. *A rigorous numerical method for the scattering from two scatterers*

Let us consider two scatterers (with homogeneous media) embedded in an homogeneous medium as depicted in Figure 1(c). The use of the integral equations discretized by the MoM leads to the linear system $\bar{\mathbf{Z}}\mathbf{X} = \mathbf{b}$, in which $\bar{\mathbf{Z}}$ is the impedance matrix of the scene made up of the two scatterers, $\mathbf{b}$ the incident field, and $\mathbf{X}$ the current on both the scatterers (the field and its normal derivative on the surfaces). The E-PILE method was developed in order to solve such a linear system efficiently and rigorously. Indeed, by inverting by block the impedance matrix and using the method of [26,28], it can be shown after some manipulations that the current $\mathbf{X}_1$ on the surface S_1 of scatterer 1 is:

$$\mathbf{X}_1 = \sum_{p=0}^{p=P_{\mathrm{PILE}}} \mathbf{Y}_1^{(p)}, \tag{1}$$

in which

$$\begin{cases} \mathbf{Y}_1^{(0)} = \bar{\mathbf{Z}}_1^{-1}\left(\mathbf{b}_1 - \bar{\mathbf{Z}}_{21}\bar{\mathbf{Z}}_2^{-1}\mathbf{b}_2\right) & \text{for } p = 0 \\ \mathbf{Y}_1^{(p)} = \bar{\mathbf{M}}_{c,1}\mathbf{Y}_1^{(p-1)} & \text{for } p > 0, \end{cases} \tag{2}$$

$\bar{\mathbf{M}}_{c,1}$ being the characteristic matrix of the scene (the two scatterers) defined as $\bar{\mathbf{M}}_{c,1} = \bar{\mathbf{Z}}_1^{-1}\bar{\mathbf{Z}}_{21}\bar{\mathbf{Z}}_2^{-1}\bar{\mathbf{Z}}_{12}$, and $\mathbf{b}_1$ the incident field illuminating the scatterer 1. $\bar{\mathbf{Z}}_1$ and $\bar{\mathbf{Z}}_2$ are the impedance matrices of scatterer 1 and scatterer 2, respectively, whereas $\bar{\mathbf{Z}}_{12}$ and $\bar{\mathbf{Z}}_{21}$ can be interpreted as coupling matrices between the two scatterers. The mathematical expressions of these matrices can be found in [26–28]. In Equation (1), the sum is truncated at order P_{PILE} obtained from a convergence criterion. By substituting subscripts {1, 2, 12, 21} for subscripts {2, 1, 21, 12} in Equations (1) and (2), the unknowns on the surface S_2, $\mathbf{X}_2$, can be found.

The physical interpretation of the characteristic matrix $\bar{\mathbf{M}}_{c,1}$ is shown in Figure 2. $\bar{\mathbf{Z}}_1^{-1}$ accounts for the local interactions on the surface S_1, so $\mathbf{Y}_1^{(0)}$ (zeroth-order term) corresponds to the current on the surface of scatterer 1 when it is illuminated by the direct incident field ($\mathbf{b}_1$) and the direct scattered field by the surface S_2 ($-\bar{\mathbf{Z}}_{21}\bar{\mathbf{Z}}_2^{-1}\mathbf{b}_2$). Indeed, $\bar{\mathbf{Z}}_2^{-1}$ accounts for the local interactions on the lower surface, and $\bar{\mathbf{Z}}_{21}$ propagates the field on the surface S_2 toward scatterer 1. In the first-order term, $\mathbf{Y}_1^{(1)} = \bar{\mathbf{M}}_{c,1}\mathbf{Y}_1^{(0)}$, $\bar{\mathbf{Z}}_{12}$ propagates the current on the surface S_1, $\mathbf{Y}_1^{(0)}$, toward the scatterer 2, $\bar{\mathbf{Z}}_2^{-1}$ accounts for the local interactions on S_2, and $\bar{\mathbf{Z}}_{21}$ re-propagates the resulting contribution toward scatterer 1; finally, $\bar{\mathbf{Z}}_1^{-1}$ updates the current values on S_1. So, the characteristic matrix $\bar{\mathbf{M}}_{c,1}$ propagates the field between the two scatterers in a back and forth manner. So, the order P_{PILE} of the E-PILE method corresponds to the number of back and forths between the scatterers.

In conclusion, the E-PILE method permits us to compute rigorously the scattering from two scatterers. Each one can be either a closed surface, like a dielectric or conducting object, or an open surface like a dielectric or conducting rough surface (three cases are depicted in Figure 1). Moreover, one of the advantages of the E-PILE method is that the resolution of the linear system $\bar{\mathbf{Z}}\mathbf{X} = \mathbf{b}$ is reduced to

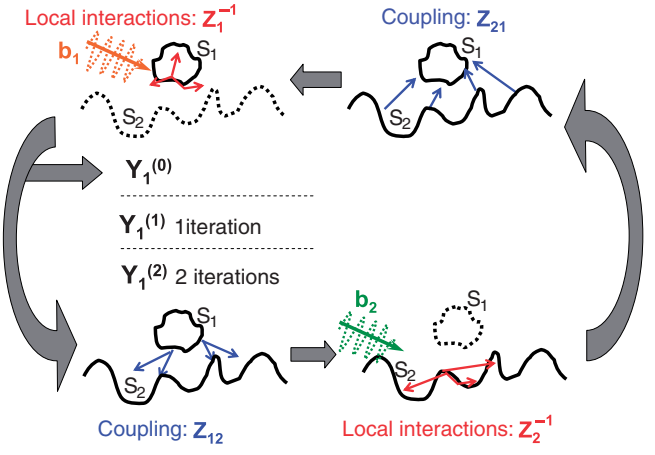

Figure 2. (Color online) Illustration of the physical interpretation of the E-PILE method.

an iterative scheme which involves the inverses of the impedance matrix of each surface. Consequently, if one of the scatterers is a rough surface (as in the cases depicted in Figure 1), the computation of the local interactions on this surface (inversion of $\bar{\mathbf{Z}}_2$ and computation of the matrix–vector product $\bar{\mathbf{Z}}_2^{-1}\mathbf{u}$, where $\mathbf{u}$ is a vector) can be realized by using a fast numerical method that already exists for scattering from a single rough surface (without the object). So, the FB-SA method [23] can be used to accelerate the E-PILE method.

2.2. *Acceleration of E-PILE by using the FB-SA*

The FB-SA method [23] is based on the FB method [22] in which the local interactions are split into forward and backward contributions leading to an iterative procedure. With spectral acceleration, the local interactions (forward and backward contributions) are split into strong and weak interactions. The strong ones are computed exactly, whereas the weak ones are computed approximately by using a spectral decomposition of the Green's function. The key parameters of the FB-SA are then the order P_{FB} involved in the iterative scheme of the FB and the strong interaction length (horizontal distance separating the weak interactions from the strong ones) x_{d0} involved in the SA. For more details, see [22–24,26,27].

The field scattered from the scene (object above a rough surface) in the far-field region (at a distance r') at the scattering angle θ_s, $\psi_s(\theta_s)$, is computed by using the Huygens principle; the fields and their normal derivatives on the surfaces (object and sea surface) are obtained from E-PILE+FB-SA. Then, the Normalized Radar Cross-Section (NRCS) of the scene is expressed as

$$\sigma(\theta_s) = \frac{r'\left|\psi_s(\theta_s)\right|^2}{2\eta_0 P_i}, \tag{3}$$

in which r' is the distance separating the scene from the receiver, $\eta_0 = 120\pi$, and P_i is the Thorsos incident power on the mid-plane of the rough surface given in [17].

3. Convergence of E-PILE combined with FB-SA

3.1. *Convergence of the FB-SA for a sea-like rough surface*

As seen before, one of the advantages of the E-PILE method is to separate the local interactions of the rough surface and those of the object. Thus, a means to obtain the parameters P_{FB} and x_{d0} is to study the scattering from a *single* rough surface (without the object). This work was investigated in [27,28] for PC (Perfectly Conducting) and dielectric 'Gaussian' (i.e. obeying a Gaussian spectrum) rough surfaces. In this paper, a rough sea surface is considered. This implies that the height of the rough surface z_2 is assumed to be a Gaussian stationary stochastic process with zero mean value as in [27,28], but the height spectrum obeys the Elfouhaily et al. hydrodynamic spectrum [29], in which the key parameter is the wind speed u_{10} at 10 meters above the sea surface. Moreover, the sea surface at radar microwave frequencies can be considered as highly conducting. Consequently, the E-PILE+FB-SA method is adapted to this case by using the IBC (Impedance Boundary Condition) approximation. This reduces the problem to a linear combination of the PC cases in TE and TM polarizations for which E-PILE+FB-SA is applied as seen in Section 2. The criterion to obtain the order P_{FB} is the same as in [28], i.e. that the Relative Residual Error (RRE) is smaller than a threshold chosen equal to 10^{-2}, where the RRE is given by

$$\mathrm{RRE} = \frac{\mathrm{norm}(\boldsymbol{\sigma} - \boldsymbol{\sigma}_{\mathrm{LU}})}{\mathrm{norm}(\boldsymbol{\sigma}_{\mathrm{LU}})} \tag{4}$$

in which 'norm' corresponds to the Euclidean norm of a vector, and $\boldsymbol{\sigma}$ and $\boldsymbol{\sigma}_{\mathrm{LU}}$ are the vectors which contain the NRCS versus the scattering angle obtained from the method under test (FB or FB-SA) and the classic MoM (with direct LU inversion: MoM+LU), respectively. In this paper, we consider $\theta_s \in]-90^\circ; +90^\circ[$ and the angle step is 0.5° for all RRE calculus.

By using this criterion, one can obtain the order P_{FB} for the case of a sea-like surface and Table 1 presents this order P_{FB} for TE and TM polarizations. It is

Table 1. Order P_{FB} with the criterion $\mathrm{RRE} < 10^{-2}$ for the TE and TM polarizations, for $f = \{3, 5\}$ GHz, for $u_{10} = \{5, 10\}\,\mathrm{m\,s^{-1}}$ and versus three different incidence angles θ_i. Sampling step $\lambda_0/10$, $N_2 = 4000$ and $g = L_2/6$.

f & u_{10} \ θ_i	0° TE-TM	30° TE-TM	60° TE-TM
3 GHz & $5\,\mathrm{m\,s^{-1}}$	4-1	4-1	5-1
3 GHz & $10\,\mathrm{m\,s^{-1}}$	4-1	4-1	5-2
5 GHz & $5\,\mathrm{m\,s^{-1}}$	4-1	4-1	5-1
5 GHz & $10\,\mathrm{m\,s^{-1}}$	4-1	4-1	5-2

computed for one surface realization. The wind speed for the Elfouhaly spectrum [29] is $u_{10} = \{5, 10\}$ m s^{-1}, the frequency is $f = \{3, 5\}$ GHz, the relative permittivity of the sea is $\varepsilon_{r2} = 70.4 + 40.6i$ for $f = 3$ GHz and $\varepsilon_{r2} = 69.2 + 35.7i$ for $f = 5$ GHz, and three different incidence angles are considered: $\theta_i = \{0^\circ, 30^\circ, 60^\circ\}$. The surface length is $L_2 = 400\lambda_0$, the sampling step is $\Delta_{x_2} = \lambda_0/10$ ($N_2 = 4000$) and Thorsos wave parameter is $g = L_2/6$.

First, we notice that the FB method converges more rapidly in TM polarization than in TE polarization. The order P_{FB} is not very sensitive to the wind speed u_{10}, the frequency and the incidence angle.

Physically, in the spatial domain, the strong interaction length defines the length around a given point where the surface is illuminated by this point: the associated waves are propagated. The weak interaction domain is related to the shadowed zone: the associated waves are not propagated (evanescent waves). From the optical point of view, the illuminated and shadowed zones are defined from the surface profile, and especially from the abscissa locations of the extrema. Thus, the horizontal distance x_{d0} (strong interaction length) separating the weak from the strong interactions is statistically related to the surface height correlation length L_c. Simulations done in previous papers [27,28] confirm this remark. In [28], the study of the convergence of FB-SA has shown that the parameter x_{d0} can be chosen equal to αL_c where L_c is the correlation length of the 'Gaussian' surface and with $\alpha = 3$. In this paper, a similar study is done but with a sea-like surface. For this case, we assume that $x_{d0} = \alpha L_c$ in which the correlation length (corresponding to gravity waves) is $L_c = 0.154 u_{10}^{2.04}$ for a sea-like surface [31]. In order to determine the value of α which provides good convergence of the FB-SA, the RRE of the FB is compared

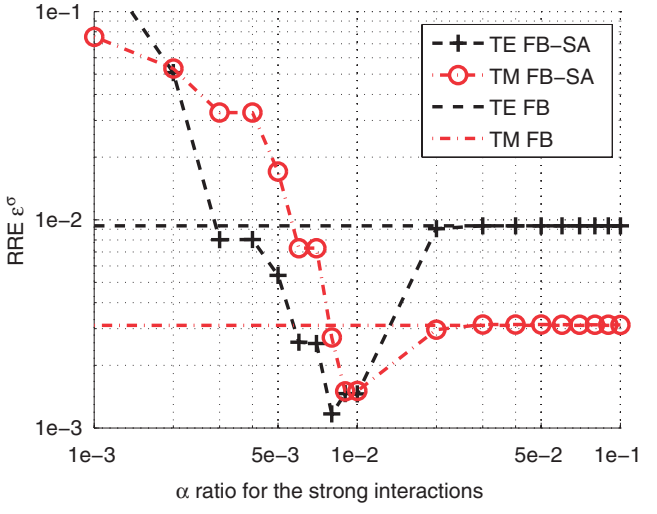

Figure 3. (Color online) Relative Residual Error of the FB and FB-SA methods versus the α ratio for TE and TM polarizations. $\Delta x = \lambda_0/10$, $N_2 = 4000$ samples, $g = L_2/6$, $f = 3$ GHz, $\theta_i = 30^\circ$, $P_{\mathrm{FB}} = \{4, 1\}$ for the {TE, TM} case.

with that of the FB-SA versus the α ratio and for TE and TM polarizations. This comparison is depicted in Figure 3. The same surface as in Table 1 is considered ($L_2 = 400\lambda_0$, $\Delta_{x_2} = \lambda_0/10$ ($N_2 = 4000$) and $g = L_2/6$) and $f = 3$ GHz (so $L_2 = 40$ m) with $\theta_i = 30^\circ$: $\varepsilon_{r2} = 70.4 + 40.6i$. The order P_{FB} is obtained from Table 1: $P_{\mathrm{FB}} = 4$ for the TE case and $P_{\mathrm{FB}} = 1$ for the TM case.

Since α is a ratio which modifies the strong interaction length, only the RRE of the FB-SA varies according to α. From $\alpha = 0.02$, the RRE of the FB-SA is equal to the FB one. The same conclusion was obtained by considering various simulations with other wind speeds, incidence angles and frequencies. So, the convergence of the FB-SA method is obtained from $\alpha = 0.02$ whereas for a Gaussian spectrum, $\alpha = 3$. Indeed, in [27], it was shown by means of physical considerations that x_{d0} must be of the order of the surface height correlation length L_c, and simulations permit us to obtain the value $\alpha = 3$. In this paper, we show for a sea surface that $x_{d0} = 0.02L_c$. This could signify that the strong interaction length is not related to the correlation length corresponding to gravity waves but to the correlation length corresponding to capillarity waves. To our knowledge, this is the first time that such a result has been shown for the FB-SA method.

Now, let us focus on the convergence of the FB-SA method according to the truncation of the sea spectrum. Indeed, the sea spectrum is truncated at low frequencies (gravity waves) at $k_{\min} = 2\pi/L_2$, and truncated at high frequencies (capillarity waves) at $k_{\max} = 2\pi/\Delta x_2$. With a sampling step $\Delta x_2 = \lambda_0/10$, we set $k_{\max} = 20\pi/\lambda$. In [32], a criterion is given to insure that the generated surface spectrum can be assimilated to the theoretical one (the inferior boundary reaches the value of 10^{-5} of the maximum): $k_{\min} \leq 0.28k_{\mathrm{pic}}$ in which $k_{\mathrm{pic}} = \Omega^2 g/u_{10}^2$ is the wavenumber of the most energetic wave. $\Omega = 0.84$ for a fully developed sea and $g = 9.81\,\mathrm{m\,s^{-2}}$. Thus, with $u_{10} = 5\,\mathrm{m\,s^{-1}}$, $k_{\mathrm{pic}} = 0.2769\,\mathrm{rad\,m^{-1}}$ which implies $k_{\min} \leq 0.0775\,\mathrm{rad\,m^{-1}}$ and then $L_2 \geq 81.0465$ m. So, with $L_2 < 81$ m the sea spectrum is truncated at low frequencies: some gravity waves are ignored. Such a sea surface length implies a high number of unknowns at microwave frequencies. For example, with $f = 3$ GHz and $L_2 = 81$ m, the number of unknowns on the sea surface (with a sampling step $\lambda_0/10 = 0.01$ m) is $N_2 = 8100$: this problem cannot be solved by using MoM+LU with a standard computer. In Table 2, the RRE of the FB and the FB-SA

Table 2. RRE versus the length of the sea surface and for the FB and the FB-SA for TE and TM polarization. $f = 1$ GHz, $u_{10} = 5\,\mathrm{m\,s^{-1}}$ ($0.28k_{\mathrm{pic}} = 0.0775$), sampling step $\lambda_0/10$, $\theta_i = 0^\circ$ and Thorsos wave parameter $g = L_2/6$. Moreover, the corresponding values of N_2 and $k_{\min}$ are reported.

Method \ L_2	3 m	15 m	30 m	120 m
N_2	100	500	1000	4000
$k_{\min}$ ($\mathrm{rad\,m^{-1}}$)	2.0944	0.4189	0.2094	0.0524
FB (TE case)	0.0033	0.0035	0.0036	0.0035
FB-SA (TE case)	0.0033	0.0035	0.0035	0.0034
FB (TM case)	0.0000	0.0000	0.0000	0.0000
FB-SA (TM case)	0.0000	0.0000	0.0000	0.0003

methods for the TE and TM cases are given versus the sea surface length with $f = 1\,\text{GHz}$: $\varepsilon_{r2} = 76 + 70i$, $u_{10} = 5\,\text{m s}^{-1}$ and $\theta_i = 0^\circ$. Four lengths are considered: $L_2 = 3\,\text{m}$, $L_2 = 15\,\text{m}$, $L_2 = 30\,\text{m}$ and $L_2 = 120\,\text{m}$. The corresponding values of N_2 and $k_{\min}$ are also listed in the table. The criterion is satisfied only for $L_2 = 120\,\text{m}$. By considering the results obtained previously in this section, an order $P_{\text{FB}} = \{5, 2\}$ for {TE, TM} polarization and a ratio $\alpha = 0.05$ are considered.

From Table 2, we can see that FB and FB-SA converge whatever the truncation of the sea spectrum since the RRE is smaller than the threshold (10^{-2}). Moreover, the errors are quite similar (for a given polarization) and not very sensitive to the length of the sea surface: the convergence of these accelerated methods does not seem to be sensitive to the truncation of the spectrum. This conclusion is consistent with another one given in [28]: the convergence of these methods are not very sensitive to the root mean square height. This numerical study shows the stability of FB and FB-SA according to the sea spectrum and the length of the sea surface.

In the following, by considering the results shown in this section, an order $P_{\text{FB}} = \{5, 2\}$ for {TE, TM} polarization and a ratio $\alpha = 0.05$ are chosen in order to insure the good convergence of FB-SA, whatever the considered scene. For example, with this ratio, the strong interaction length is only $x_{d0} = 0.2\,\text{m}$ with $u_{10} = 5\,\text{m s}^{-1}$. So, the main conclusion of this study is that the FB-SA method is particularly interesting for maritime applications.

3.2. *Convergence of E-PILE + FB-SA for a canonical object above a sea-like rough surface*

In this section, the convergence of E-PILE+FB-SA is studied for scattering from perfectly conducting canonical objects above a rough sea surface. As seen in Section 2, the E-PILE method is applied and accelerated by using FB-SA for the local interactions on the rough surface. Three scenes are considered: a circular cylinder above a sea surface, a plate above a sea surface and a cross above a sea surface. These three canonical objects are depicted in Figure 4.

For each scene, $f = 3\,\text{GHz}$: $\varepsilon_{r2} = 70.4 + 40.6i$, $u_{10} = 5\,\text{m s}^{-1}$, $L_2 = 400\lambda_0 = 40\,\text{m}$, $\Delta_{x_2} = \lambda_0/10$ ($N_2 = 4000$), $g = L_2/6$, and $\theta_i = 30^\circ$. TE polarization is considered. From the study in Section 3.1, we set $P_{\text{FB}} = 4$ and $\alpha = 0.05$ ($x_{d0} = 0.2\,\text{m}$). The circular cylinder has a radius $a = 2.5\lambda_0 = 0.25\,\text{m}$ and is described by $N_1 = 157$ samples. The

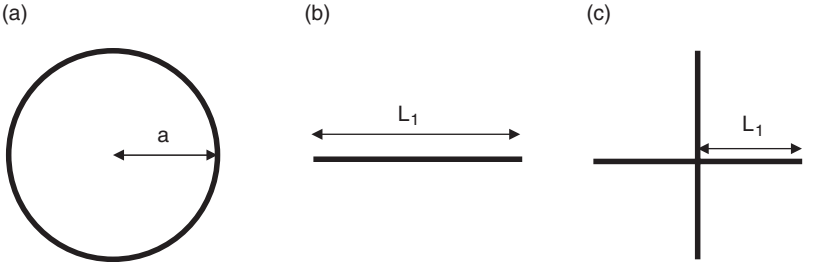

Figure 4. Three canonical objects: a cylinder (a), a plate (b) and a cross (c).

Table 3. RRE versus the order P_{PILE} for the TE polarization and for three canonical objects above a rough surface. $f = 5\,\mathrm{GHz}$, $u_{10} = 5\,\mathrm{m\,s^{-1}}$, sampling step $\lambda_0/10$, $N_2 = 4000$ samples and Thorsos wave parameter $g = L_2/6$, $\theta_i = 30^\circ$.

Object \ P_{PILE}	0	1	2	3
cylinder	0.0835	0.0348	0.0089	0.0080
plate	0.1793	0.0176	0.0115	0.0084
cross	0.1231	0.0201	0.0082	0.0080

plate has a length $L_1 = 5\lambda_0 = 0.50\,\mathrm{m}$, described by $N_1 = 100$ samples and oriented horizontally as in Figure 4(b). The cross is made up of four plates with $L_1 = 2.5\lambda_0 = 0.25\,\mathrm{m}$; it is described by $N_1 = 200$ samples and oriented in such a manner that two plates are oriented horizontally and the other two are oriented vertically, as in Figure 4(c). Consequently, these three canonical objects are circumscribed in a circle with a diameter $D = 0.50\,\mathrm{m}$. The center of each object is located at $(x_0 = -h_0 \tan(\theta_i),\ h_0 = 20\lambda_0 = 2\,\mathrm{m})$ in such a way that each object is centered on the Thorsos wave. One surface realization is considered. The convergence criterion to obtain the order P_{PILE} is to insure the RRE (of E-PILE+FB-SA) is smaller than 10^{-2}. Table 3 presents the RRE obtained from E-PILE+FB-SA for the three scenes and versus the order P_{PILE}.

From Table 3, as the order P_{PILE} increases, the RRE decreases. Indeed, the order P_{PILE} corresponds to the number of back and forths between the object and the sea surface, so the coupling is more taken into account with a high order P_{PILE}. From $P_{\mathrm{PILE}} = 2$, E-PILE+FB-SA converges (under the criterion $\mathrm{RRE} < 10^{-2}$) for the cylinder and the cross above the sea surface and from $P_{\mathrm{PILE}} = 3$, E-PILE+FB-SA converges for the plate above the sea surface. Thus, the convergence is only slightly sensitive to the shape of the object and it is obtained very rapidly.

In Figures 5–7, the NRCS for the circular cylinder, the plate and the cross above the sea surface are depicted, respectively. For each figure, the E-PILE+FB-SA method is compared with MoM+LU (with direct LU inversion). The same parameters as in Table 3 are considered.

From Figures 5–7, one can see very good agreement between E-PILE+FB-SA and MoM+LU. If $N_2 \gg N_1$, the complexity of the direct LU inversion is $\mathcal{O}(N_2^3)$ for the computing time and $\mathcal{O}(N_2^2)$ for memory requirements. As shown in [27,28], the complexity of E-PILE+FB-SA is $\mathcal{O}(N_2)$ for both computing time and memory requirements. Consequently, the E-PILE+FB-SA method can be used to study rigorously a more realistic scene which implies a high number of unknowns.

4. Monte Carlo simulations for a cross above a sea-like rough surface

4.1. *Criterion for the convergence of E-PILE + FB-SA*

For more realistic results, the random behavior of the scene must be taken into account. This is done with the Monte Carlo process. By using a spectral method,

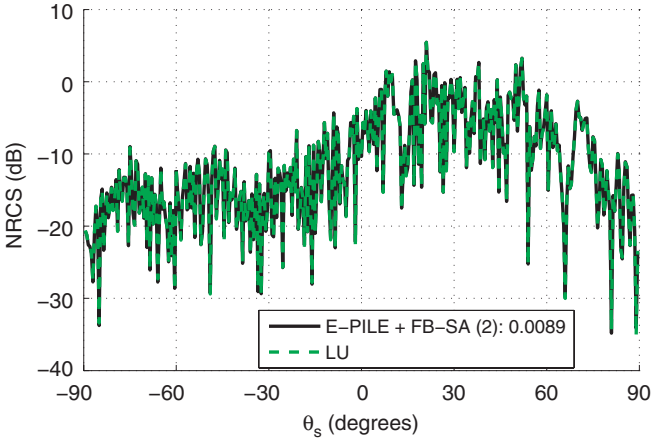

Figure 5. (Color online) Comparison of the NRCS of a cylinder above a sea surface computed from E-PILE+FB-SA with that computed from a direct LU inversion versus the scattering angle θ_s. The radius of the cylinder (see Figure 4(a)) is $a = 2.5\lambda_0 = 0.25\,\text{m}$, $N_1 = 157$, ($x_0 = -1.15\,\text{m}$, $h_0 = 2\,\text{m}$) with the same parameters as in Table 3. In the legend, the order P_{PILE} is given in parentheses and the RRE is also reported.

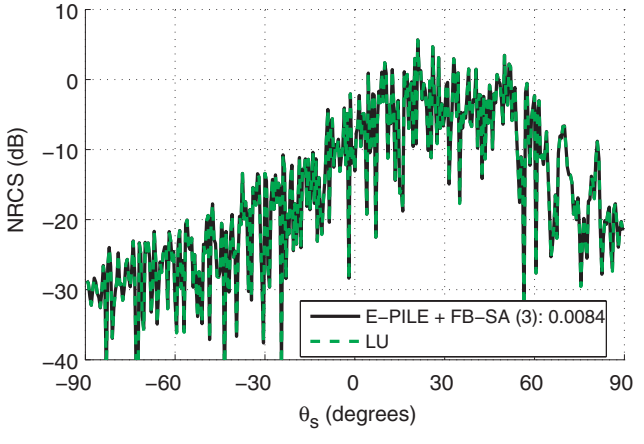

Figure 6. (Color online) Same as in Figure 5 but with a plate (see Figure 4(b)) of length $L_1 = 0.50\,\text{m}$ ($N_1 = 100$).

several independent surfaces (but with the same Gaussian process and the same height spectrum) are generated. A cross is put above each generated surface at the same position (x_0, h_0). For each scene (numbered 'r') the scattered field ψ_r is calculated from E-PILE+FB-SA to order P_{PILE} and versus the scattering angle θ_s. Then, the NRCS (total component: second uncentered moment) with the Monte Carlo process is evaluated from

$$\sigma(\theta_s, P_{\text{PILE}}) = \frac{r'\left\langle \left| \Psi_{P_{\text{PILE}}}(\theta_s) \right|^2 \right\rangle}{2\eta_0 P_i}, \tag{5}$$

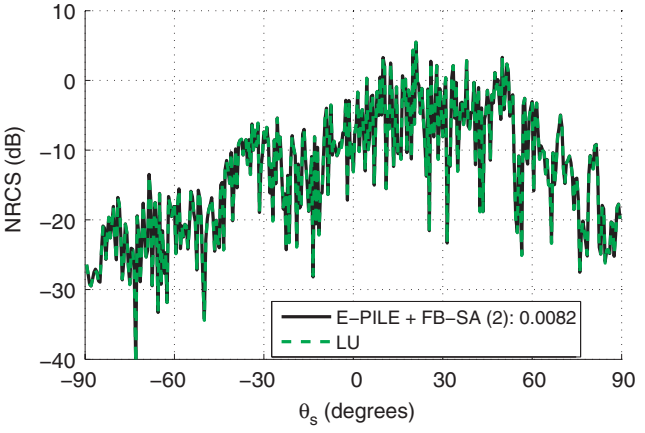

Figure 7. (Color online) Same as in Figure 5 but with a cross (see Figure 4(c)), in which each plate has a length $L_1 = 0.25\,\text{m}$ ($N_1 = 200$).

with

$$\left\langle \left| \Psi_{P_{\text{PILE}}}(\theta_s) \right|^2 \right\rangle = \frac{1}{R} \sum_{r=1}^{r=R} \left| \psi_r(\theta_s, P_{\text{PILE}}) \right|^2. \tag{6}$$

As seen previously, the higher the order P_{PILE}, the more the method E-PILE+FB-SA converges to the MoM+LU. In this paper, the authors propose a criterion to choose the order P_{PILE} which provides good convergence (called P_{conv}). The NRCS is evaluated with E-PILE+FB-SA for $P_{\text{PILE}} = \{1, 2, \ldots, P_{\max}\}$. P_{conv} is obtained with the following criterion (with $\theta_s \in [-\pi/2;\ \pi/2]$):

$$\begin{aligned} P_{\text{conv}} = \big\{ & (P_{\text{PILE}} + 1)/ \\ & \max\left(\left| \sigma_{\text{dB}}(\theta_s, P_{\text{PILE}} + 1) - \sigma_{\text{dB}}(\theta_s, P_{\text{PILE}}) \right| \right) < S_0 \big\}, \end{aligned} \tag{7}$$

in which $\max(\mathbf{x})$ provides the maximum value of the vector $\mathbf{x}$ over $\theta_s \in [-\pi/2;\ \pi/2]$, σ_{dB} represents the NRCS σ expressed in dB, and S_0 is a threshold expressed in dB. In this paper, we set $S_0 = 0.1\,\text{dB}$.

4.2. *Numerical results*

Numerical results of the NRCS (given by Equation (5)) are presented for a perfectly conducting cross located above a rough sea surface by considering 50 realizations ($R = 50$). Comparisons are done with the results obtained by considering the sea surface only (without the cross) and a cross above a flat surface. For all the results presented here: the frequency is $f = 3\,\text{GHz}$: $\varepsilon_{r2} = 70.4 + 40.6i$, $L_2 = 1000\lambda_0 = 100\,\text{m}$, $\Delta_{x_2} = \lambda_0/10$ ($N_2 = 10\,000$), and $g = L_2/6$. The cross is described by $N_1 = 800$ samples, with $L_1 = 10\lambda_0 = 1\,\text{m}$, centered on ($x_0 = -h_0 \tan(\theta_i)$, $h_0 = 2\,\text{m}$) and oriented as in Figure 4(c). In Figure 8, $u_{10} = 5\,\text{m}\,\text{s}^{-1}$, $\theta_i = 0^\circ$ and TE polarization is considered.

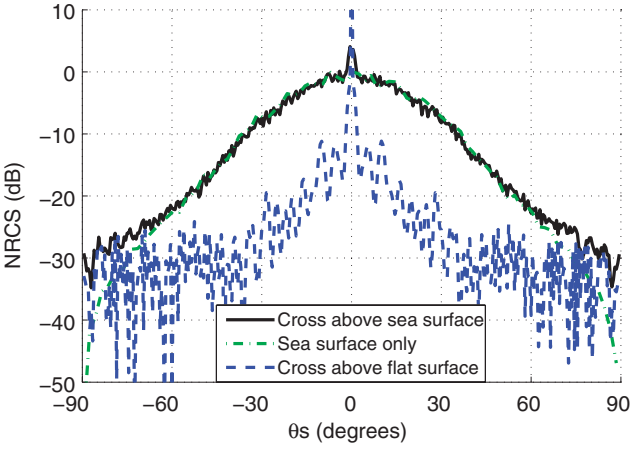

Figure 8. (Color online) Comparison of the NRCS of a cross above a sea surface with the NRCS of the sea surface only versus θ_s. In addition, the NRCS of a cross above a flat surface is given. $f = 3\,\text{GHz}$, $L_2 = 1000\lambda_0 = 100\,\text{m}$, $\Delta_{x_2} = \lambda_0/10$ ($N_2 = 10\ 000$), $g = L_2/6$, $u_{10} = 5\,\text{m s}^{-1}$, $\theta_i = 0^\circ$, TE polarization is considered. P_{conv} is given in Table 4. $L_1 = 10\lambda_0 = 1\,\text{m}$, $N_1 = 800$ and ($x_0 = 0\,\text{m}$, $h_0 = 2\,\text{m}$).

Table 4. Order P_{conv} and computing time (for one realization) for the scenes considered in Figures 8–11.

	Figure 8	Figure 9	Figure 10	Figure 11
P_{conv}	8	7	6	5
Computing time (in minutes)	9.7	9	3.4	6.7

The order P_{conv} obtained from criterion (7) is given in Table 4. Moreover, the computing time for one realization is also given. A dual core 3 GHz personal computer with 4 GB of RAM with Matlab software was used in this work.

In Figure 9, the same parameters as in Figure 8 are considered but $u_{10} = 10\,\text{m s}^{-1}$. In Figure 10, the same parameters as in Figure 8 are considered but the polarization is TM. In Figure 11, the same parameters as in Figure 8 are considered but $\theta_i = 60^\circ$. The orders P_{conv} and the computing time for these three scenes are listed in Table 4.

From Figure 8, one can see that the object could be detected if the receiver is located at grazing angles ($|\theta_s| > 70^\circ$) and in the normal direction, which corresponds to the backscattering direction ($\theta_s = \theta_i = 0^\circ$). For other scattering angles, the NRCS obtained with the cross above the sea surface is close to that obtained with the rough surface only. In Figure 9, the sea is rougher as the wind speed u_{10} increases and the object could be difficult to detect at grazing observation angles ($|\theta_s| > 70^\circ$). Indeed, the rougher the sea, the more the slopes of the surface are strong and then the further the energy is away from the specular direction (spread over π radians). Thus, the signature of the sea surface is higher than that of the object in contrast to the case

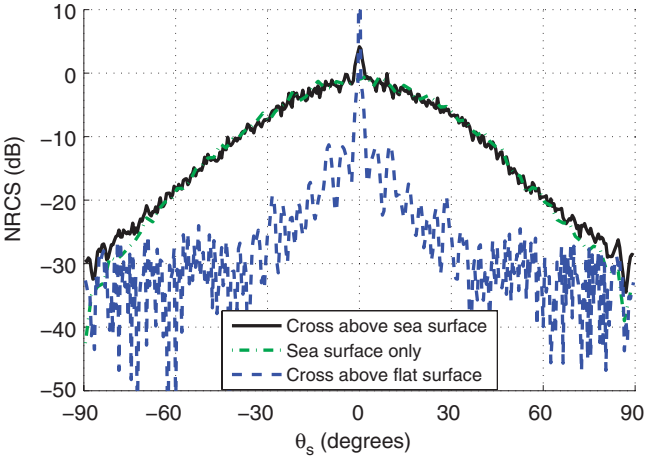

Figure 9. (Color online) Same parameters as in Figure 8 but with $u_{10} = 10\,\mathrm{m\,s^{-1}}$.

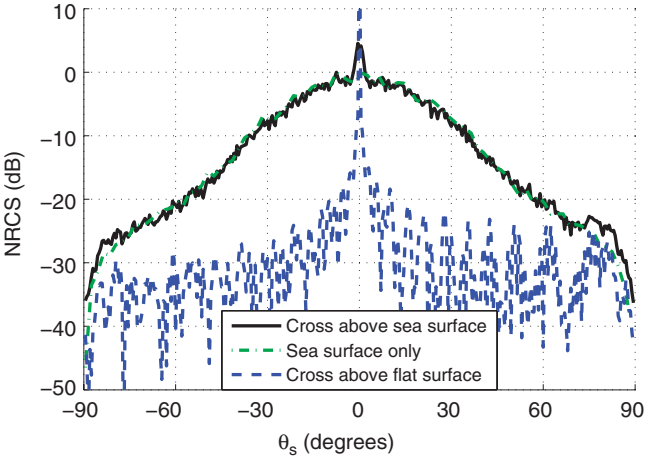

Figure 10. (Color online) Same parameters as in Figure 8 but the polarization is TM.

of Figure 8. The same conclusion can be drawn for the TM polarization with the results of Figure 10. This could mean that the detection of the object is easier in TE polarization. From Figure 11, one can see that the object can be easily detected around the backscattering direction ($\theta_s < 0°$). Indeed, the vertical plates of the cross create high backscattering NRCS due to double reflections with the horizontal plates. From Figures 8–11, one can notice that even if the object has small dimensions compared to the sea surface, it plays an important role in the signature of the scene, in particular in the specular and backscattering directions. Moreover, the roughness of the sea implies a spreading of the energy over the scattering directions whereas for the cross above a flat surface, there are privileged scattering directions.

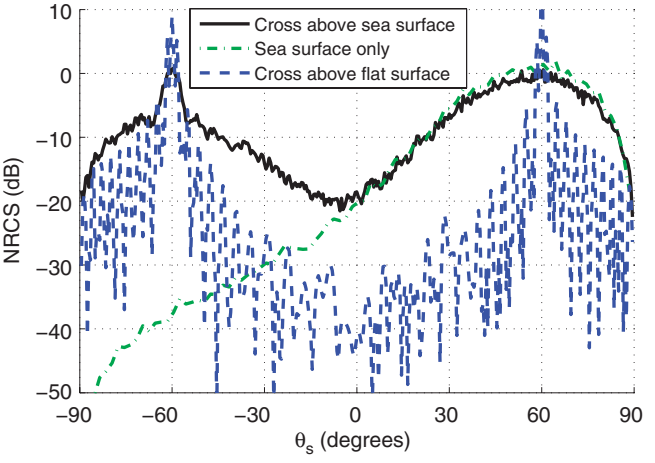

Figure 11. (Color online) Same parameters as in Figure 8 but with $\theta_i = 60^\circ$ (the cross is centered on ($x_0 = -3.46$ m, $h_0 = 2$ m)).

So, the rougher the sea, the more the object can be difficult to detect by considering the total component of the NRCS. With a rougher sea surface, the coherent component of the NRCS could be used in order to improve the detection. It is computed from the following equation:

$$\sigma^{\mathrm{coh}}(\theta_s, P_{\mathrm{PILE}}) = \frac{r' \left| \left\langle \Psi_{P_{\mathrm{PILE}}}(\theta_s) \right\rangle \right|^2}{2\eta_0 P_i}, \tag{8}$$

with

$$\left| \left\langle \Psi_{P_{\mathrm{PILE}}}(\theta_s) \right\rangle \right|^2 = \left| \frac{1}{R} \sum_{r=1}^{r=R} \psi_r(\theta_s, P_{\mathrm{PILE}}) \right|^2. \tag{9}$$

Since it is related to the contribution of the deterministic elements of the scene, the NRCS of a single sea surface (without the object) with a strong roughness in the coherent component is low whereas the cross (deterministic object) provides a high NRCS. Thus, for a cross above a sea surface, the coherent component is closely related to the NRCS of the cross. Finally, it is important to notice that the results presented in this section cannot be obtained by using a classic MoM+LU with a standard personal computer. Indeed, if the number of unknowns on the sea surface is much greater than that object, one can show that the complexity of E-PILE+FB-SA is $\mathcal{O}(N_2)$ which permits us to compute the scattering from an object above a very long sea surface (results in [28] showed that the method can be applied with $N_2 = 100\,000$ unknowns and $N_1 = 63$ with a similar standard PC as the one used in this paper). Thus, this method can be used to study scattering from an object above a very long sea surface as, for example, for grazing incidence.

4.3. *Toward the Low Grazing Angle (LGA)*

The Thorsos wave can be applied for moderate incidence angles and allows us to remove edge diffraction. But, as detailed in [17,18], the Thorsos wave satisfies the Helmholtz equation if:

$$kg\cos(\theta_i) \gg 1. \tag{10}$$

Thus, for a constant g parameter ($g = L_2/6$ for example), the higher θ_i, the more the surface must be long. Toporkov et al. [33] explained why Kapp proposed another criterion for the applicability of the Thorsos wave at LGAs. This criterion is given by:

$$g > \frac{A\sqrt{2}}{k(\pi/2 - \theta_i)\cos(\theta_i)}, \tag{11}$$

where A is some constant. Kapp proposed the value $A = 3$, whereas Toporkov et al. used $A = 6.64$ to insure good physical results (a Pierson–Moskowitz spectrum was considered in their study) [33]. With $\theta_i = 85^\circ$, $f = 3\,\text{GHz}$, and $A = 6.64$, from Equation (11), $g > 19.6499\,\text{m}$, and $L_2 > 117.8993\,\text{m}$ with $g = L_2/6$.

Let us study the normal derivative of the field $|\partial\psi_2/\partial n_2|$ on the sea surface, by considering a single rough sea surface (without object). One surface realization is considered. The polarization is TE, $g = L_2/6$, $\theta_i = 85^\circ$, $f = 3\,\text{GHz}$ and $u_{10} = 5\,\text{m s}^{-1}$. The currents $|\partial\psi_2/\partial n_2|$ are plotted versus the abscissa x in Figure 12(a), (b) and (c) for $L_2 = 70\,\text{m}$ (the Kapp criterion with the Toporkov value of A is not satisfied), $L_2 = 117.9\,\text{m}$ (the criterion is only just satisfied) and for $L_2 = 400\,\text{m}$ (the criterion is fully satisfied), respectively.

From Figure 12(a), (b) and (c), we can observe that with $L_2 = 400\,\text{m}$, physical results are obtained since the currents on the surface go down near the edges of the surface: the Kapp criterion (with the Toporkov value of A) is satisfied. For $L_2 = 117.9\,\text{m}$, the currents go down more slowly at the right edge: the criterion is only just satisfied. For $L_2 = 70\,\text{m}$, the currents seem to be constant at the right edge: the Kapp criterion with the Toporkov value of A is not satisfied. These results are consistent with the Toporkov conclusions.

Now, let us study the normal derivative of the field $|\partial\psi_2/\partial n_2|$ on the sea surface, by considering a cross above a rough sea surface. The polarization is TE, $g = L_2/6$, $\theta_i = 85^\circ$, $f = 3\,\text{GHz}$, $u_{10} = 5\,\text{m s}^{-1}$, $L_1 = 10\lambda_0 = 1\,\text{m}$, $N_1 = 800$ and ($x_0 = -22.86\,\text{m}$, $h_0 = 2\,\text{m}$). In Figure 13(a), (b) and (c), the currents $|\partial\psi_2/\partial n_2|$ are plotted versus the abscissa x for $L_2 = 70\,\text{m}$, $L_2 = 117.9\,\text{m}$ and $L_2 = 400\,\text{m}$, respectively. For each case, P_{conv} is given in Table 5.

We observe that for $L_2 = 400\,\text{m}$ and $L_2 = 117.9\,\text{m}$, physical results are obtained since the currents on the surface go down near the edges of the surface. But for $L_2 = 70\,\text{m}$, non-physical current behavior is observed (high values at the left edge). In addition, scattering from the cross (by direct reflection and also by coupling) induces higher levels of currents on the sea surface edges than those obtained from a single sea surface (comparison between Figures 13(c) and 12(c), for example). Thus, the presence of the cross above the sea surface makes the use of the Thorsos wave more restrictive. Indeed, if the incident wave does not satisfy the Helmholtz equation, the

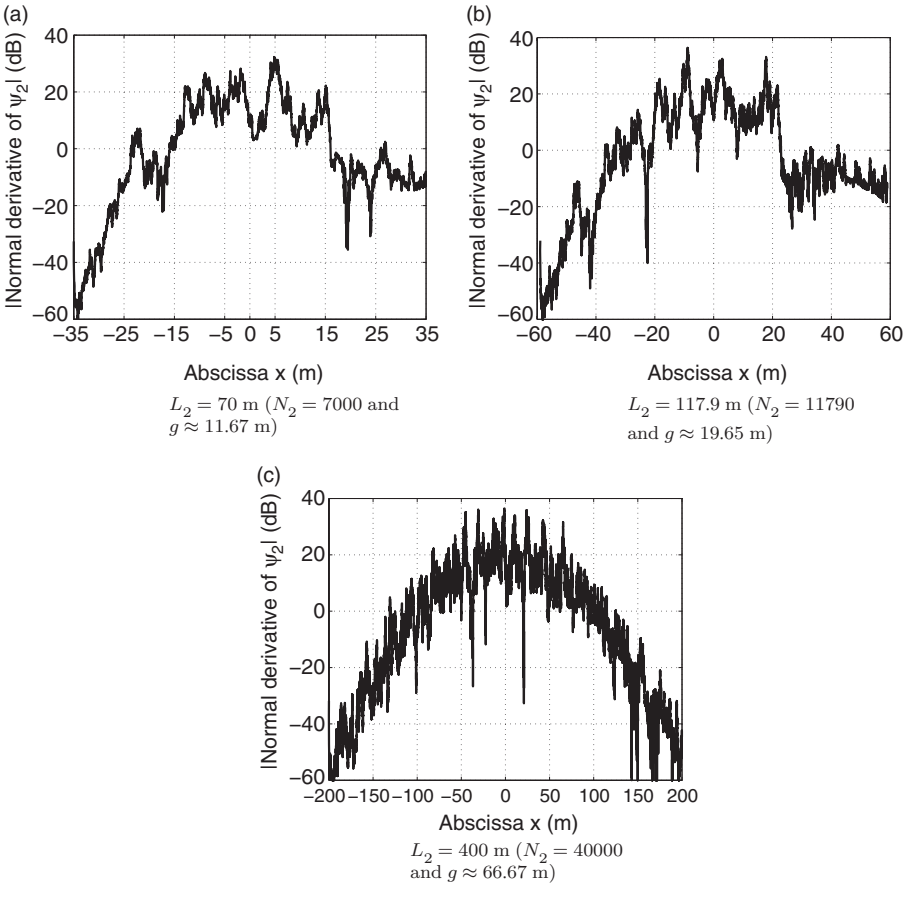

Figure 12. Normal derivative of the field $|\partial\psi_2/\partial n_2|$ on the sea surface (without object) with $L_2 = 70\,\text{m}$, $L_2 = 117.9\,\text{m}$ and $L_2 = 400\,\text{m}$. TE polarization is considered, $g = L_2/6$, $\theta_i = 85^\circ$, $f = 3\,\text{GHz}$ and $u_{10} = 5\,\text{m s}^{-1}$.

non-physical phenomena are propagated between the two surfaces owing to the coupling.

In Figure 14, a comparison of the NRCS for a single rough sea surface (without object) for the three different surface lengths is plotted versus θ_s with the same parameters as in Figure 12. Fifty realizations are considered for the Monte Carlo process.

In Figure 15, the comparison of the NRCS for the cross above the sea surface for the three different surface lengths is also plotted versus θ_s. The same parameters as in Figure 13 are considered. The order P_{conv} and the computing time for each surface length is given in Table 5.

In spite of the fact that, for the single sea surface, the currents were very different according to the length of the sea surface (comparison of Figure 12(a), (b) and (c)),

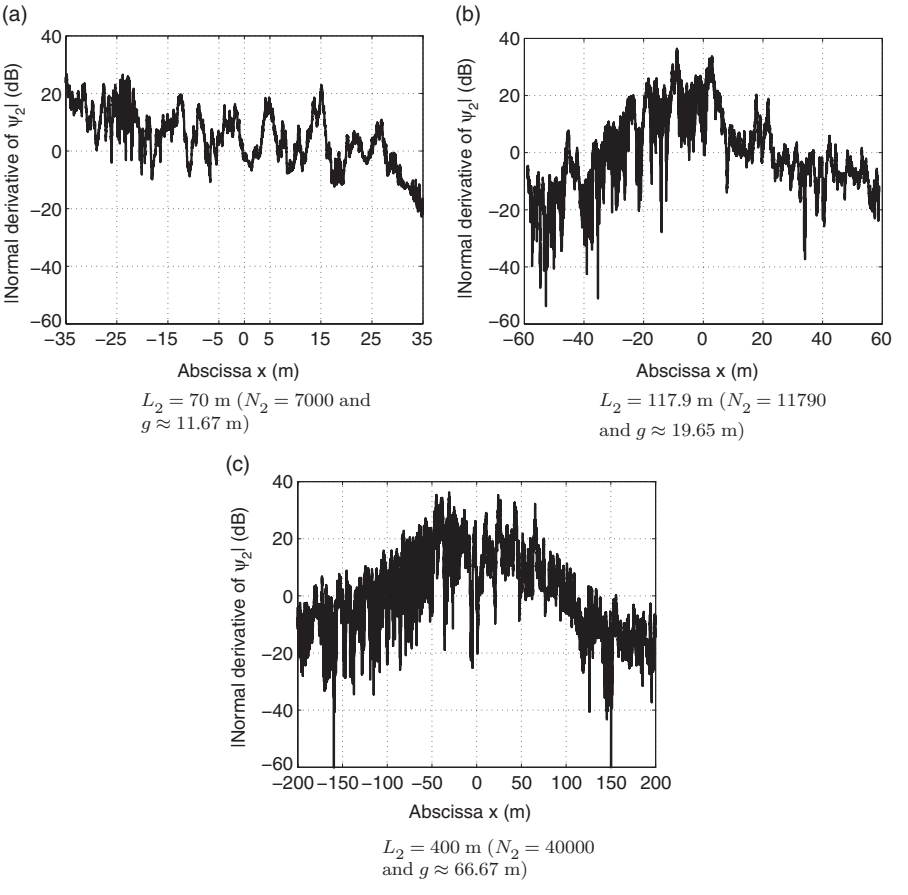

$L_2 = 70$ m ($N_2 = 7000$ and $g \approx 11.67$ m)

$L_2 = 117.9$ m ($N_2 = 11790$ and $g \approx 19.65$ m)

$L_2 = 400$ m ($N_2 = 40000$ and $g \approx 66.67$ m)

Figure 13. Same as in Figure 12 but with a cross above the sea surface with $L_1 = 10\lambda_0 = 1$ m, $N_1 = 800$ and ($x_0 = -22.86$ m, $h_0 = 2$ m).

Table 5. Order P_{conv} and computing time (for one realization) for the scenes considered in Figure 15.

	$L_2 = 70$ m	$L_2 = 117.9$ m	$L_2 = 400$ m
P_{conv}	7	6	6
Computing time (in minutes)	3.6	10	90.4

the NRCS for these three sea surfaces (see Figure 14) are similar. Thus, the Kapp criterion with the Toporkov value of A seems to be too restrictive. Nevertheless, these results are in agreement with the study done by Ye et al. [34]. Indeed, from their charts, we found (with another criterion) $g > 87\lambda$ for $\theta_i = 85^\circ$ and then $L_2 \geq 325\lambda$, which implies $L_2 \geq 32.5$ m for $f = 3$ GHz. Thus, for more accurate results, particularly

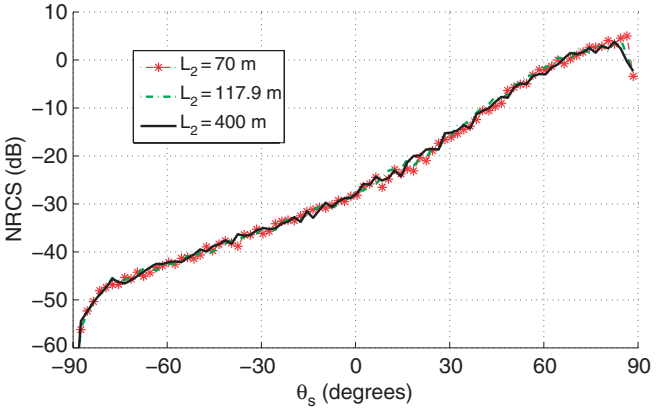

Figure 14. (Color online) Comparison of the NRCS of a single rough sea surface with $L_2 = 70$ m, $L_2 = 117.9$ m and $L_2 = 400$ m. Same parameters as in Figure 12 with 50 realizations.

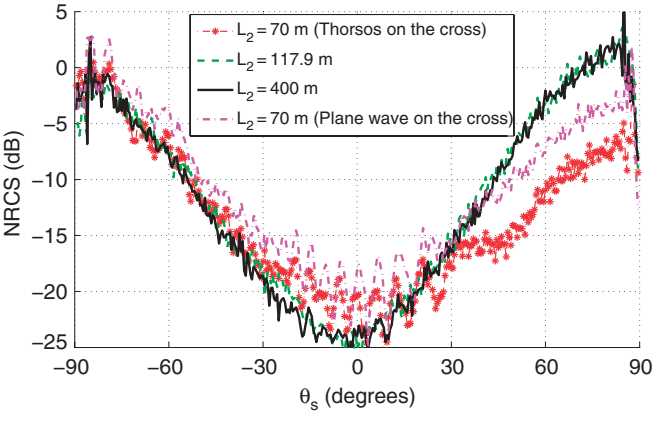

Figure 15. (Color online) Comparison of the NRCS of the cross above a sea surface with $L_2 = 70$ m, $L_2 = 117.9$ m and $L_2 = 400$ m. Same parameters as in Figure 13 with 50 realizations.

for the currents, the Kapp criterion with the Toporkov value of A must be used; but for good NRCS results, a smaller sea surface is sufficient according to the Ye criterion.

For the case of the cross above the sea surface, physical results are obtained for $L_2 = 117.9$ m and $L_2 = 400$ m (similar behavior of the NRCS for the two lengths) in Figure 15. As for the results obtained in Figure 11, the object can easily be detected around the backscattering direction ($\theta_s < 0°$) (comparison between Figures 14 and 15). Indeed, the double reflections of the cross (reflections between the vertical plates and the horizontal ones) and the coupling between the cross and the sea surface provide a high backscattering NRCS. But for $L_2 = 70$ m, different behavior is obtained, in particular near the specular direction ($\theta_s = 85°$). As said before, the presence of the cross above the sea surface makes the use of the Thorsos wave more restrictive, and then the Ye criterion [34] is not valid for this scene.

As shown previously, for LGA, the validity of the Thorsos wave becomes questionable (it becomes a non-physical wave). In order to investigate this point, one can apply a plane wave only for the object illumination. In the E-PILE algorithm, in Equation (2), $\mathbf{b}_2$ (the incident field on the sea surface) is computed from the Thorsos wave equation, whereas $\mathbf{b}_1$ (the incident field on the cross) is computed from the plane wave equation. The NRCS, obtained with this excitation substitution and with $L_2 = 70\,\mathrm{m}$, is depicted in Figure 15. Even if this process may also be questionable (the incident wave on the object is different from that for the sea surface, especially in terms of phase), it permits us to obtain quite good results. Indeed, one can observe that the results are globally more accurate with this excitation (plane wave on the object) than when the Thorsos wave is used both on the sea surface and on the object. In spite of the fact that some non-physical oscillations appear near $\theta_s = 0^\circ$ (there are no oscillations on the other curves), the results are 5 dB better near the specular direction for a plane wave on the object.

To our knowledge, there is no study of a criterion of the Thorsos wave for an object above a rough sea surface. In fact, this parametrization is quite complex since it depends on the shape of the object and its location above the sea. Further investigations like those made by Toporkov et al. [33] and Ye et al. [34] could be undertaken for an object above the sea (with the Elfouhaily hydrodynamic spectrum). This is not the scope of this paper. Other further work could be performed on the use of a recently published approach in order to suppress edge effects without using a tapered wave [35]. Another solution to avoid these problems for LGA could be to find and to define a new tapered wave valid for such a configuration.

5. Conclusion

In this paper, the scattering from canonical objects above a sea-like one-dimensional rough surface is investigated. Since such a problem cannot be solved easily with a classical Method of Moments (with direct LU inversion), a recently developed fast numerical method called E-PILE is used. This allows us to use the Forward–Backward Spectral Acceleration (FB-SA) for the computation of local interactions on the sea surface. A convergence criterion is proposed to determine the order P_{FB} and the strong interaction length involved in the FB-SA method. This study leads to a new conclusion: for a sea-like surface, the strong interaction length could be related to the correlation length corresponding to the capillarity waves. Thus, the FB-SA is particularly interesting for a maritime context. Then, the convergence of E-PILE+FB-SA is investigated for the scattering from a canonical object (cylinder, plate and cross) located above a sea surface. This study leads to an important conclusion: E-PILE+FB-SA can be considered as a benchmark method whatever the shape of the object. Indeed, although the three objects imply different scattering mechanisms, the E-PILE+FB-SA method converges to MoM+LU very rapidly. Since $N_2 \gg N_1$, the complexity of this approach is $\mathcal{O}(N_2)$ which permits us to compute the scattering from an object above a very long sea surface. Thus, this method is appropriate for a maritime application at microwave frequencies, for

which the MoM+LU cannot be used with a standard personal computer. Finally, the case of low grazing incidence is studied.

Acknowledgements

The authors would like to thank Dr J.V. Toporkov for useful comments and remarks on low grazing angles. This work was supported by the French defence procurement agency DGA (Délégation Générale pour l'Armement) under REI Grant 2008.34.0041.

References

[1] A. Madrazo and M. Nieto-Vesperinas, *Scattering of light and other electromagnetic waves from a body buried beneath a highly rough random surface*, J. Opti. Soc. Amer. 14 (1997), pp. 1859–1866.

[2] D.E. Lawrence and K. Sarabandi, *Electromagnetic scattering from a dielectric cylinder buried beneath a slightly rough surface*, IEEE Trans. Antennas Propagat. 50 (2002), pp. 1368–1376.

[3] X. Wang, C.-F. Wang, Y.-B. Gan, and L.-W. Li, *Electromagnetic scattering from a circular target above or below rough surface*, Prog. Electromag. Res. 40 (2003), pp. 207–227.

[4] J.T. Johnson and R.J. Burkholder, *A study of scattering from an object below a rough surface*, IEEE Trans. Geosci. Remote Sens. 42 (2004), pp. 59–66.

[5] C.-H. Kuo and M. Moghaddam, *Electromagnetic scattering from a buried cylinder in layered media with rough interfaces*, IEEE Trans. Antennas Propagat. 54 (2006), pp. 2392–2401.

[6] Y. Altuncu, A. Yapar, and I. Akduman, *On the scattering of electromagnetic waves by bodies buried in a half-space with locally rough interface*, IEEE Trans. Geosci. Remote Sens. 44 (2006), pp. 1435–1443.

[7] M.R. Pino, L. Landesa, J.L. Rodriguez, F. Obelleiro, and R. Burkholder, *The generalized Forward–Backward method for analyzing the scattering from targets on ocean-like rough surfaces*, IEEE Trans. Antennas Propagat. 47 (1999), pp. 961–969.

[8] M.R. Pino, R. Burkholder, and F. Obelleiro, *Spectral acceleration of the generalized Forward–Backward method*, IEEE Trans. Antennas Propagat. 50 (2002), pp. 785–797.

[9] Z.-X. Li, *Bistatic scattering from rough dielectric soil surface with a conducting object with arbitrary closed contour partially buried by using the FBM/SAA method*, Prog. Electromag. Res. 76 (2007), pp. 253–274.

[10] Y. Zhang, Y.E. Yang, H. Braunisch, and J.A. Kong, *Electromagnetic wave interaction of conducting object with rough surface by hybrid SPM/MoM technique*, Prog. Electromag. Res. 22 (1999), pp. 315–335.

[11] J.T. Johnson and R.J. Burkholder, *Coupled canonical grid/discrete dipole approach for computing scattering from objects above or below a rough interface*, IEEE Trans. Geosci. Remote Sens. 39 (2001), pp. 1214–1220.

[12] J.T. Johnson, *A numerical study of scattering from an object above a rough surface*, IEEE Trans. Antennas Propagat. 50 (2002), pp. 1361–1367.

[13] P. Liu and Y.Q. Jin, *The finite-element method with domain decomposition for electromagnetic bistatic scattering from the comprehensive model of a ship on and a target above a large scale rough sea surface*, IEEE Trans. Geosci. Remote Sens. 42 (2004), pp. 950–956.

[14] H. Ye and Y. Jin, *Fast iterative approach to difference electromagnetic scattering from the target above a rough surface*, IEEE Trans. Geosci. Remote Sens. 44 (2006), pp. 108–115.
[15] H. Ye and Y.-Q. Jin, *A hybrid analytic-numerical algorithm of scattering from an object above a rough surface*, IEEE Trans. Antennas Propagat. 45 (2007), pp. 1174–1180.
[16] L.-X. Guo, A.-Q. Wang, and J. Ma, *Study on EM scattering from 2D target above 1-D large scale rough surface with low grazing incidence by parallel MoM based on PC clusters*, Prog. Electromag. Res. 89 (2009), pp. 149–166.
[17] L. Tsang, J.A. Kong, K.-H. Ding, and C.O. Ao, *Scattering of Electromagnetics Waves: Volume II. Numerical Simulations*. *Wiley Series on Remote Sensing*, John Wiley, New York, 2001.
[18] E.I. Thorsos, *The validity of the Kirchhoff approximation for rough surface scattering using a Gaussian roughness spectrum*, J. Acoust. Soc. Amer. 83 (1988), pp. 78–92.
[19] L. Tsang, C.H. Chang, and H. Sangani, *A Banded Matrix Iterative Approach to Monte Carlo simulation of scattering of waves by large scale random rough surface problems: TM case*, Electron. Lett. 29 (1993), pp. 1666–1667.
[20] L. Tsang, C.H. Chang, H. Sangani, A. Ishimaru, and P. Phu, *A Banded Matrix Iterative Approach to Monte Carlo simulations of large scale random rough surface scattering: TE case*, J. Electromag. Waves Appl. 29 (1993), pp. 1185–1200.
[21] D. Kapp and G. Brown, *A new numerical method for rough-surface scattering calculations*, IEEE Trans. Antennas Propagat. 44 (1996), pp. 711–722.
[22] D. Holliday, L.L. DeRaad Jr, and G.J. St-Cyr, *Forward–Backward: a new method for computing low-grazing angle scattering*, IEEE Trans. Antennas Propagat. 44 (1996), pp. 722–729.
[23] H.T. Chou and J.T. Johnson, *A novel acceleration algorithm for the computation of scattering from rough surfaces with the Forward–Backward method*, Radio Sci. 33 (1998), pp. 1277–1287.
[24] D. Holliday, L.L. DeRaad Jr, and G.J. St-Cyr, *Forward–Backward for scattering from imperfect conductor*, IEEE Trans. Antennas Propagat. 46 (1998), pp. 101–107.
[25] H.T. Chou and J.T. Johnson, *Formulation of Forward–Backward method using Novel Spectral Acceleration for the modeling of scattering from impedance rough surfaces*, IEEE Trans. Geosci. Remote Sens. 38 (2000), pp. 605–607.
[26] N. Déchamps, N. De Beaucoudrey, C. Bourlier, and S. Toutain, *Fast numerical method for electromagnetic scattering by rough layered interfaces: Propagation-Inside-Layer Expansion method*, J. Opti. Soc. Amer.A 23 (2006), pp. 359–369.
[27] C. Bourlier, G. Kubické, and N. Déchamps, *A fast method to compute scattering by a buried object under a randomly rough surface: PILE combined with FB-SA*, J. Opti. Soc. Amer.A 25 (2008), pp. 891–902.
[28] G. Kubické, C. Bourlier, and J. Saillard, *Scattering by an object above a randomly rough surface from a fast numerical method: extended PILE method combined with FB-SA*, Wave. Random Complex 18 (2008), pp. 495–519.
[29] T. Elfouhaily, B. Chapron, K. Katsaros, and D. Vandermark, *A unified directional spectrum for long and short wind-driven waves*, J. Geophys. Res. 102 (1997), pp. 781–796.
[30] W. Ellison, A. Balana, G. Delbos, K. Lamkaouchi, L. Eymard, C. Guillou, and C. Prigent, *New permittivity measurements of seawater*, Radio Sci. 33 (1998), pp. 639–648.
[31] C. Bourlier and G. Berginc, *Microwave analytical backscattering models from randomly rough anisotropic sea surface – comparison with experimental data in C and Ku bands*, Prog. Electromag. Res. 37 (2002), pp. 31–78.
[32] C. Bourlier, J. Saillard, and G. Berginc, *Intrinsec infrared radiation of the sea surface*, Prog. Electromag. Res. 27 (2000), pp. 185–335.

[33] J.V. Toporkov, R.S. Awadallah, and G.S. Brown, *Issues related to the use of a Gaussian-like incident field for low-grazing-angle scattering*, J. Opti. Soc. Amer. A 16 (1999), pp. 176–187.

[34] H. Ye and Y.-Q. Jin, *Parametrization of the tapered incident wave for numerical simulation of electromagnetic scattering from rough surface*, IEEE Trans. Antennas Propagat. 53 (2005), pp. 1234–1237.

[35] P. Spiga, G. Soriano, and M. Saillard, *Scattering of electromagnetic waves from rough surfaces: A boundary integral method for low-grazing angles*, IEEE Trans. Antennas Propagat. 56 (2008), pp. 2043–2050.